Icarus 197 (2008) 505–518

Contents lists available at ScienceDirect

Icarus

www.elsevier.com/locate/icarus

Galileo observations of volcanic plumes on Io

P.E. Geissler [a,*], M.T. McMillan [b]

[a] U.S. Geological Survey, 2255 N. Gemini Dr., Flagstaff, AZ 86001, USA
[b] Northern Arizona University, S. San Francisco St., Flagstaff, AZ 86011, USA

ARTICLE INFO

Article history:
Received 15 May 2006
Revised 28 April 2008
Available online 29 May 2008

Keywords:
Io
Volcanism

ABSTRACT

Io's volcanic plumes erupt in a dazzling variety of sizes, shapes, colors and opacities. In general, the plumes fall into two classes, representing distinct source gas temperatures. Most of the Galileo imaging observations were of the smaller, more numerous Prometheus-type plumes that are produced when hot flows of silicate lava impinge on volatile surface ices of SO_2. Few detections were made of the giant, Pele-type plumes that vent high temperature, sulfur-rich gases from the interior of Io; this was partly because of the insensitivity of Galileo's camera to ultraviolet wavelengths. Both gas and dust spout from plumes of each class. Favorably located gas plumes were detected during eclipse, when Io was in Jupiter's shadow. Dense dust columns were imaged in daylight above several Prometheus-type eruptions, reaching heights typically less than 100 km. Comparisons between eclipse observations, sunlit images, and the record of surface changes show that these optically thick dust columns are much smaller in stature than the corresponding gas plumes but are adequate to produce the observed surface deposits. Mie scattering calculations suggest that these conspicuous dust plumes are made up of coarse grained "ash" particles with radii on the order of 100 nm, and total masses on the order of 10^6 kg per plume. Long exposure images of Thor in sunlight show a faint outer envelope apparently populated by particles small enough to be carried along with the gas flow, perhaps formed by condensation of sulfurous "snowflakes" as suggested by the plasma instrumentation aboard Galileo as it flew through Thor's plume [Frank, L.A., Paterson, W.R., 2002. J. Geophys. Res. (Space Phys.) 107, doi:10.1029/2002JA009240. 31-1]. If so, the total mass of these fine, nearly invisible particles may be comparable to the mass of the gas, and could account for much of Io's rapid resurfacing.

Published by Elsevier Inc.

1. Introduction

Io's explosive volcanic eruptions are among the most spectacular but least well understood phenomena in the Solar System. These violent eruptions take place when volatile vapors are expelled from volcanoes at speeds of up to 1000 m per second, forming plumes of gas and dust that reach hundreds of kilometers above the satellite's surface. Only a few of Io's many active volcanoes have been observed to produce plumes, and another handful of volcanic centers have been inferred to have plume activity through observations of the surface changes caused by deposits emplaced by plumes. Several of Io's plumes have apparently been sustained for decades, while others erupted in episodic big bangs that lasted less than a few weeks.

Voyager and Galileo observations have established that there are two classes of plumes on Io (McEwen and Soderblom, 1983; Geissler et al., 2004a): giant plumes like Pele[1] that vent sulfur-rich gases from the interior of the moon and spray-paint the surface with enormous red rings, and more numerous smaller plumes like Prometheus that are produced when hot flows of silicate lava impinge on volatile surface ices of SO_2. Both classes of plumes possess gas and dust components, although the density of dust and gas varies from one plume to another, even within the same class. Fallout from the plumes continually coats the surface in a constantly changing variety of colors, while the gases contribute substantially to Io's tenuous atmosphere. A fraction of the dust and gas ejected by plumes is swept away by Jupiter's magnetic field, helping to sustain the neutral clouds, plasma torus, and dust streams escaping Io.

Io's plumes were intensively studied soon after their discovery in Voyager imaging data. Strom and Schneider (1982) provided detailed observational descriptions of the plumes that were imaged by Voyagers 1 and 2. Collins (1981) estimated the dust

* Corresponding author. Fax: +1 (928) 556 7014.
E-mail address: pgeissler@usgs.gov (P.E. Geissler).

[1] Due to their variability in space and time, plumes on Io are not given names. It should be understood that references to plumes are in fact references to the specific plumes issuing from the corresponding named eruptive centers.

0019-1035/$ – see front matter Published by Elsevier Inc.
doi:10.1016/j.icarus.2008.05.005

particle size and mass of Loki's dust plume by fitting a Rayleigh scattering law to Voyager 1 color observations. Kieffer (1982) presented a thorough theoretical treatment of the thermodynamics of plumes and their possible sources. Johnson and Soderblom (1982) pointed out the importance of plumes for global resurfacing and heat flow. McEwen and Soderblom (1983) studied plume deposits and surface changes between the Voyager 1 and 2 encounters and recognized the distinction between the two classes of plumes on Io.

However, many aspects of the plumes remained mysterious until the arrival of Galileo in 1995. Still poorly known are the temporal and spatial variability of plumes, the relationship between the plumes and the surface changes they produce, and the nature and sources of the particulates present in plumes of both classes. Among the outstanding unanswered questions are the following:

- How do the plumes alter the surface of Io? Geissler et al. (2004a) documented dozens of surface changes that took place during the 5 year tenure of Galileo, and found surface changes at every location in which plumes had been spotted. Are the visible surface changes due to dust deposition from the plumes, or to condensation of gas from the plumes onto the surface?
- How are dust particles formed? Does it "snow" sulfurous flakes that are condensed as the gas expands and cools? Or are the dust particles made up of volcanic ash that is entrained with the gas flow?
- How big are the dust particles? Estimates of the dust particle radii in Io's plumes range from <10 nm (Collins, 1981) to 0.1 mm (James and Wilson, 1998), depending upon the assumptions made, an inconsistency of 4 orders of magnitude.
- How massive are the dust plumes? Published estimates of dust production rates for Io's plumes also vary greatly, ranging from 10^3 kg s^{-1} for Pele (Spencer et al., 1997) through 10^7 kg s^{-1} for both Pele and Pillan (Cataldo et al., 2002), up to 10^8 kg s^{-1} for Loki (Collins, 1981).
- How significant are volcanic plumes to Io's resurfacing? Answers to the previous questions are needed to determine whether the plumes can account for the rapid resurfacing of Io, responsible for erasing any hint of bombardment of the moon by impactors. A globally averaged resurfacing rate of $\sim$1 mm yr^{-1} is required in order to account for the burial of impact craters on Io (Spencer and Schneider, 1996), equivalent to the emplacement of 1000 m^3 s^{-1}. How much of this is due to plume deposits and how much to the emplacement of silicate lava flows is an open question.

In this article, we begin to address the above problems through a systematic study of the dimensions, colors and opacities of dust plumes in the complete set of Galileo images, together with comparisons of the dust plumes seen in daylight to the gaseous auroral glows seen in eclipse and the record of surface changes. In the following sections we first outline our measurement methodologies before presenting the Galileo data on the sizes and morphologies of dust and gas plumes, and the colors and scattering behavior of the Prometheus-type dust plumes for which numerous observations exist. Next we interpret the color data using Mie theory to derive constraints on dust particle sizes, and apply these constraints to estimate the masses of the dust plumes and the corresponding mass production rates. Finally we discuss the implications of the results for the genesis of dust in Io's plumes, revisit the importance of the plumes for global resurfacing, outline the deficiencies in our knowledge of Io's plumes, and suggest directions for further research.

2. Approach

Galileo Solid State Imaging (SSI) pictures of Io's plumes were acquired with a mix of different geometries, resolutions, phase angles, and compression ratios. Many of these images were captured in targeted campaigns specifically intended to monitor plume activity on Io (McEwen et al., 1998; Keszthelyi et al., 2001; Turtle et al., 2004). To analyze these data, the images were first imported into the USGS ISIS software system (Gaddis et al., 1997), navigated (camera pointing corrected), and radiometrically calibrated using the procedures of Klaasen et al. (1997) to either reflectance units (I/F) or spectral radiance (nW cm^{-2} sr^{-1} nm^{-1}). Individual frames of the color observations were coregistered and assembled into color cubes so that all of the filters could be measured simultaneously.

The heights of dust columns were measured in sunlit images of plumes, correcting for the foreshortening that occurs when the plume is in front of or behind the limb. The correction was calculated by first finding the angle by which the plume was rotated around from the limb using the cosine formula of spherical trigonometry with the known latitudes and longitudes of the subspacecraft point and the source of the plume, where the plume source location was based on the tabulation of surface changes from Geissler et al. (2004a). Then a plane cosine correction was applied to derive the true dust column heights from the measured heights.

The heights of gas plumes were measured in eclipse images with a similar foreshortening correction applied. Galileo images of Io in eclipse show many different diffuse glows associated with various components of the atmosphere and electrical currents stimulating the emissions (Geissler et al., 1999, 2001a, 2004b). Only very massive or favorably located plumes (near the sub-Jupiter and anti-Jupiter points of Io) produce visible auroral emissions that could be detected by Galileo's SSI camera. For this study, we measured the heights of gas plumes if they met two criteria: (1) distinct knots of emission with discernable plume morphology, and (2) association with a clearly identifiable volcanic center known to have produced surface changes.

The brightness and color of the sunlit dust plumes were measured as functions of phase angle and corrected for residual calibration errors by subtracting the average values of the dark space background surrounding the plumes. The dust plume brightness (I/F) is strongly affected by the position of the plume with respect to Io's limb, and the sparse Galileo data do not allow us to reliably quantify the scattering phase function of the dust. However, the color observations are self-consistent when normalized to the Violet filter brightness, and these measurements are discussed in Section 3.7.

The total optical power scattered by the sunlit dust plumes was estimated as the product of the mean measured spectral radiance (nW cm^{-2} sr^{-1} nm^{-1}) times the solid angle per pixel (1.03×10^{-10} sr for Full Frame mode, 4.13×10^{-10} sr for Summation mode), times the number of pixels subtended by the plume, times the filter bandwidth (45 nm for Violet images; 65 nm for Green).

3. Observations

Almost all of the Galileo plume sightings were of the smaller, more common Prometheus-type plumes. Only two images detected giant, Pele-type plumes, and these are discussed separately in Section 3.5. All of the Galileo plume images were acquired at low resolution ($>$1.6 km/pixel), comparable to the pictures of plumes taken by the Voyagers. An attempt to image Prometheus at 45 m/pixel during orbit I31 unfortunately failed due to a camera anomaly (Turtle et al., 2004). Because of severe telemetry

Table 1
Dust plume heights

Name	Type	Lat.	Lon.	Orbit	Image	Filter	GMT (M/D/Y H:M)	Res. (km/pix)	Meas. height (km)	Meas. error (km)	Corr. height (km)	Corr. error (km)	Position/notes
Grian	Pe	−12	13	C10	s0413791600	Red	9/19/1997 20:49	10.5	84.2	30	144	51	Limb
Kanehekili	Pr	−19	34	G8	s0394435001	Violet	5/6/1997 22:52	13.0	70.2	13	75	14	Limb
Kanehekili	Pr	−16	36	E11	s0420900323	Violet	11/8/1997 18:45	19.5	100.7	20	101	20	Limb
Masubi	Pr	−44	54	C21	s0506406118	Violet	7/2/1999 4:04	2.6	82.2	20	87	21	Limb
Masubi	Pr	−44	54	C21	s0506406153	Violet	7/2/1999 4:05	3.3	91.0	10	96	11	Limb
Masubi	Pr	−44	54	C21	s0506406800	Green	7/2/1999 4:11	1.6	74.9	10	80	11	Limb
Masubi	Pr	−44	54	C21	s0506584123	Violet	7/3/1999 10:04	16.7	93.9	20	99	21	Limb
Masubi	Pr	−44	54	C22	s0512352501	Violet	8/12/1999 22:09	10.8	63.1	20	64	20	Limb
Masubi	Pr	−44	54	C22	s0512375600	Violet	8/13/1999 2:02	12.8	64.0	20	92	29	Limb
Masubi	Pr	−44	54	I31	s0615693301	Violet	8/7/2001 12:58	19.6	61.4	20	91	30	Limb
Masubi	Pr	−44	54	I31	s0615816301	Violet	8/8/2001 9:42	19.9					Terminator
Amirani	Pr	21	112	C22	s0512420523	Violet	8/13/1999 9:37	15.9	36.6	15	66	27	Limb
Amirani	Pr	21	112	C22	s0512436223	Violet	8/13/1999 12:15	16.4	73.6	15	76	15	Limb
Amirani	Pr	21	112	C22	s0512447723	Violet	8/13/1999 14:12	16.5	36.8	20	87	47	Limb
Amirani	Pr	23	115	E4	s0374850023	Violet	12/20/1996 10:27	18.3	40.4	20	72	36	Limb
Amirani	Pr	24	116	G8	s0394478123	Violet	5/7/1997 6:09	9.8	52.8	15	60	17	Limb
Thor	Pr	39	131	I31	s0615325147	Violet	8/4/2001 22:56	18.3	103.3	18	107	19	Limb
Thor	Pr	39	131	I31	s0615325547	Violet	8/4/2001 23:00	18.2	120.0	10	123	10	Limb
Prometheus	Pr	−1	155	G2	s0359402500	Violet	9/2/1996 23:15	30.8					Terminator
Prometheus	Pr	−1	155	G2	s0359653300	Violet	9/4/1996 17:31	21.9					Terminator
Prometheus	Pr	−1	155	G2	s0359722942	Violet	9/5/1996 5:15	18.7	56.5	20	86	30	Limb
Prometheus	Pr	−1	155	G2	s0359729642	Violet	9/5/1996 6:23	19.0	76.1	20	76	20	Limb
Prometheus	Pr	−1	155	G2	s0359736542	Violet	9/5/1996 7:33	19.3	38.9	20	67	35	Limb
Prometheus	Pr	−1	155	C3	s0368558239	Clear	11/6/1996 6:10	3.5					Disk
Prometheus	Pr	−1	155	E4	s0374575922	Violet	12/19/1996 12:15	11.7					Disk
Prometheus	Pr	−1	155	E6	s0383600826	Violet	2/19/1997 21:07	10.9					Terminator
Prometheus	Pr	−1	155	G8	s0394435001	Violet	5/6/1997 22:52	13.0					Terminator
Prometheus	Pr	−1	155	G8	s0394505123	Violet	5/7/1997 10:41	10.0	89.9	10	90	10	Limb
Prometheus	Pr	−1	155	C9	s0401785407	Violet	6/27/1997 13:33	8.3	66.4	16	71	17	Limb
Prometheus	Pr	−1	155	C9	s0401863204	Violet	6/28/1997 2:40	6.2	295.7	60	74	15	Disk
Prometheus	Pr	−1	155	C9	s0401876300	Violet	6/28/1997 4:52	12.7					Terminator
Prometheus	Pr	−1	155	E11	s0420730085	Violet	11/7/1997 14:05	9.3	68.2	10	79	12	Limb
Prometheus	Pr	−1	155	E11	s0420789285	Violet	11/8/1997 0:03	8.0					Terminator
Prometheus	Pr	−1	155	C21	s0506492200	Violet	7/2/1999 18:34	10.0					Terminator
Prometheus	Pr	−1	155	C22	s0512466924	Violet	8/13/1999 17:26	16.3	48.9	20	72	29	Limb
Prometheus	Pr	−1	155	C22	s0512475823	Violet	8/13/1999 18:56	16.1	58.5	15	59	15	Limb
Zamama	Pr	18	171	G1	s0349673978	Violet	6/26/1996 15:49	13.9	75.3	15	79	16	Limb
Zamama	Pr	18	172	G8	s0394519124	Violet	5/7/1997 13:03	10.5	61.0	20	62	20	Limb
Zamama	Pr	19	175	E11	s0420730085	Violet	11/7/1997 14:05	9.3	29.6	10	80	27	Limb
Zamama	Pr	19	175	E11	s0420743485	Violet	11/7/1997 16:20	9.0	66.1	20	67	20	Limb
Zamama	Pr	19	175	E11	s0420789285	Violet	11/8/1997 0:03	8.0					Disk
Zamama	Pr	18	176	E14	s0440873652	Violet	3/29/1998 0:37	3.0					Disk
Zamama	Pr	18	176	I24	s0520873452	Violet	10/11/1999 18:05	6.7					Terminator
Marduk	Pr	−23	211	G8	s0394552545	Violet	5/7/1997 18:41	11.4	51.0	20	52	20	Limb
Marduk	Pr	−23	211	E11	s0420773085	Violet	11/7/1997 21:19	8.2	76.0	8	76	8	Limb
Marduk	Pr	−25	212	C21	s0506405768	Violet	7/2/1999 4:01	2.9	32.9	10	92	28	Limb
Pillan	Pr	−11	242	C9	s0401863204	Violet	6/28/1997 2:40	6.2	99.3	20	109	22	Limb
Pillan	Pr	−12	243	E11	s0420789285	Violet	11/8/1997 0:03	8.0	105.4	25	118	28	Limb
Pele	Pe	−18	255	E4	s0374850023	Violet	12/20/1996 10:27	18.3	180.9	20	426	47	Limb
Pele	Pe	−18	255	G29	s0584334178	Violet	12/31/2000 8:23	10.3	297	30	299	30	Limb
Ra	Pr	−10	323	G1	s0350024288	Violet	6/29/1996 2:50	9.9	91.8	10	104	11	Limb

constraints, the Galileo SSI images were subjected to a lossy compression that produced blocky artifacts, particularly near the limb where plumes are most easily seen. The compression algorithm preserved the low spatial frequencies and the mean of each 8×8 pixel block, so the lossy compression does not affect the quantitative results presented below.

3.1. Dust plume sizes

Table 1 lists our inventory of Galileo images of dust plumes that were detected in daylight. Over the course of the 5 year mission, Galileo acquired 51 observations of sunlit plumes from 11 different volcanic centers. The best Galileo images of these plumes are presented in Fig. 1. In general, the Prometheus-type dust columns appeared similar to one another in size and shape but varied considerably in opacity and color. Fig. 1 shows that the Prometheus-type dust plumes displayed a characteristic fountain- or umbrella-shaped morphology with a dense central column, contrasting with the shieldlike shapes of giant plumes that lack a dense core.

Kanehekili (Fig. 1A) was seen twice in 1997 in color observations taken during orbits G8 and E11. Plume sightings at Kanehekili are consistent with the record of surface changes (Geissler et al., 2004a), which suggest a reduced level of activity in the last half of the Galileo mission. Masubi (Fig. 1B) was not spotted until 1999, but was imaged at the highest spatial resolution of any of the Galileo era plumes. The images of Masubi from orbit C21 show a cone-shaped core with sharp margins, surrounded by a diffuse envelope of dust. Amirani (Fig. 1C) was active from late 1996 through 1999 but was only seen by Galileo from great distances. Thor (Fig. 1D) erupted unexpectedly late in the mission in 2001; the observations of Thor were intended to capture an expected eruption of Tvashtar. In contrast, Prometheus (Fig. 1E) was dependably present throughout the Galileo mission and has likely been erupting since the Voyager flybys. Zamama (Fig. 1F) was active during most of the mission, but was not detected in the tar-

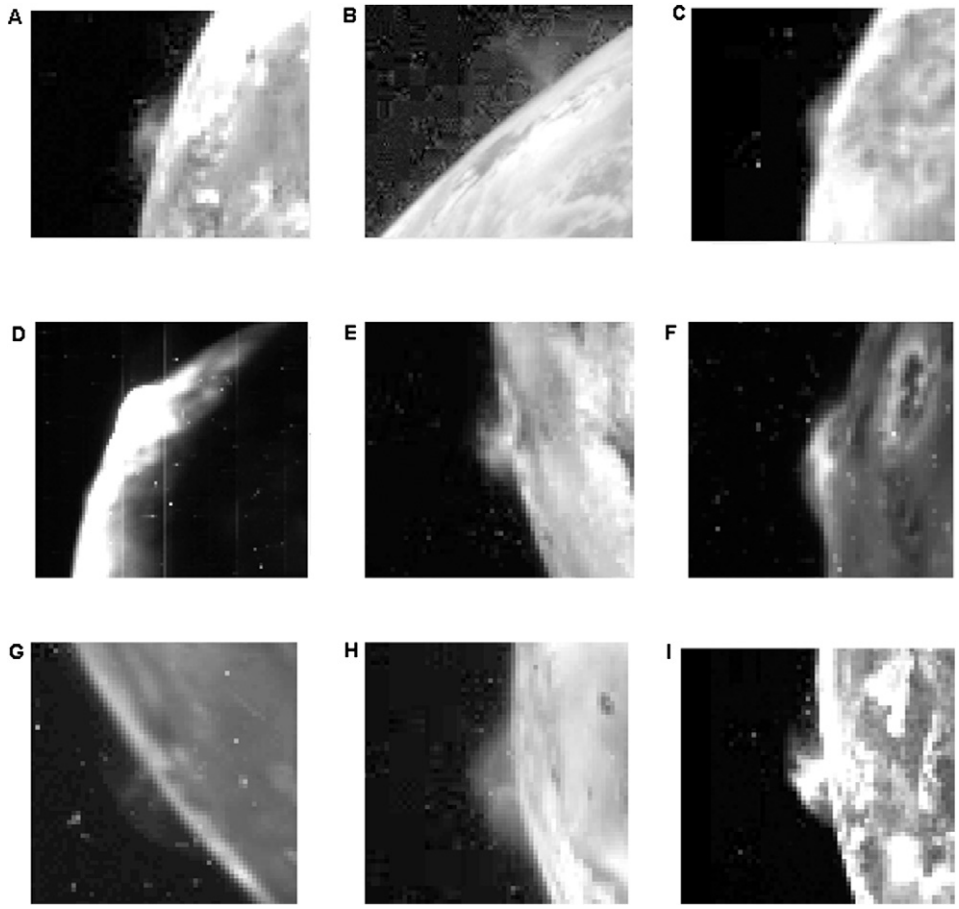

Fig. 1. Galileo images of sunlit Prometheus-type plumes. The Prometheus-type dust plumes display a characteristic fountain- or umbrella-shaped morphology with a dense central column, contrasting with the shieldlike shapes of giant plumes that lack a dense core. (A) Kanehekili orbit G8 (image s0394435001), (B) Masubi C21 (s0506406153), (C) Amirani C22 (s0512436223), (D) Thor I31 (s0615325147), (E) Prometheus E11 (s0420730085), (F) Zamama E11 (s0420743485), (G) Marduk E11 (s0420773085), (H) Pillan C9 (s0401863204), (I) Ra G1 (s0350024288).

geted plume search conducted during orbits C21 and C22. Marduk (Fig. 1G) was rarely spotted by Galileo and was always faint when it was seen. The surface changes at Marduk were also very subtle. Pillan (Fig. 1H) had a single episodic eruption that produced a conspicuous black deposit superimposed on Pele's red ring. Ra (Fig. 1I) was spotted only once at the beginning of the Galileo mission. Not included in Table 1 are Maui, Loki, and Volund that were seen by the Voyagers but plume activity at these locations apparently ceased between 1981 and 1996. The giant plume from Tvashtar was seen in ultraviolet observations by Cassini, along with Pele's dust plume. Many other active plumes were missed by Galileo's camera but revealed themselves through surface changes or SO_2 frost deposits (Geissler et al., 2001b, 2004a; Doute et al., 2001). Culann and Acala were both prominent in eclipse images taken by Galileo (next section) but were never detected during daylight, suggesting that dust was largely absent from these "stealth" plumes (Johnson et al., 1995).

Many of the plume sightings were made when the plumes were near the terminator or over the disk of Io, but 38 observations took place when plumes were near enough to the limb to enable accurate height determinations to be made. Fig. 2 shows a histogram of these dust column height measurements. In this and subsequent histograms, the frequency on the vertical axis refers to the number of observations, not the number of distinct plumes from different volcanic centers. Corrected heights of the Prometheus-type dust columns range from 52 km to 123 km, with a mean of 82 km and a standard deviation of 17 km. Not included in this calculation are the giant plumes Pele and Grian or the faint outer plume of Thor, about which we will have more to say later. Of the Prometheus-type dust plumes, only Pillan, Ra and Thor reached over 100 km in height. Repeated observations showed no temporal variability in dust column heights beyond the measurement uncertainty. The dust load varied considerably from plume to plume: no dust columns were seen at Acala and Culann, and the opacity of stealthy Marduk is an order of magnitude less than that of similarly sized Zamama (Fig. 3). However, there does not appear to be a correlation between dust plume optical depths and dust plume heights in the Galileo observations, indicating that the visible dust load of Prometheus-type plumes varies independently of the height of the plumes (which is controlled by gas temperature).

3.2. Gas plume sizes

Galileo observed auroral emissions from several favorably located plumes while Io was eclipsed in Jupiter's shadow. Because of their distinctive morphology, these plume glows can be distinguished from the variety of auroral emissions that are visible even when no plumes are present. The plume glows are stimulated by electrical currents near the sub- and anti-Jupiter points of Io, and show the extent of the gas component of the plumes. Gas plumes from Grian, Kanehekili, Ra, and Acala were all seen on the Jupiter-facing side of Io. Prometheus, Culann, and Zamama were consistently detected on the side of Io facing away from Jupiter. The shapes of these gas plumes ranged from jets to domes to amorphous glows. Table 2 lists the plumes detected in Galileo eclipse images of Io that appeared as distinct knots of emission and could

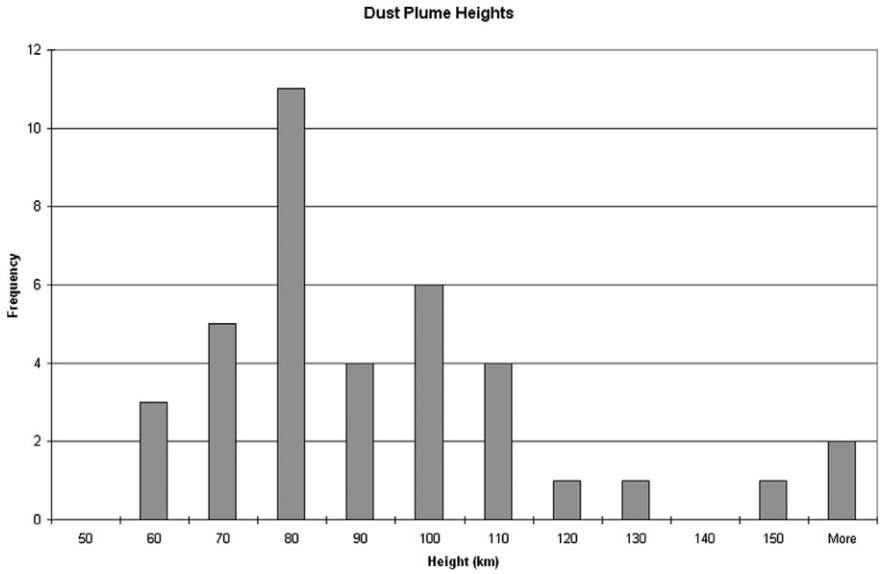

Fig. 2. Histogram of dust column heights. The frequency on the vertical axis refers to the number of observations, not the number of distinct plumes from different volcanic centers. Corrected heights of the Prometheus-type dust columns range from 52 km to 123 km, with a mean of 82 km and a standard deviation of 17 km. The outliers are Thor and Pele.

Table 2
Gas plume heights

Name	Type	Lat.	Lon.	Orbit	Image	Filter	GMT (M/D/Y H:M)	Res. (km/pix)	Meas. height (km)	Meas. error (km)	Corr. height (km)	Corr. error (km)	Position/notes
Grian	Pe	−12	13	C21	s0506570500	Clear	7/3/1999 7:46	30.2	339.8	45	506	67	Left limb
Kanehekili	Pr	−16	36	E11	s0420361523	Clear	11/4/1997 23:58	17.9	253.0	40	398	63	Left limb
Thor	Pr	39	131	I31	s0615325147	Violet	8/4/2001 22:56	18.3	440.0	30	444	30	Left limb; sunlit obs.
Thor	Pr	39	131	I31	s0615325547	Violet	8/4/2001 23:00	18.2	230.0	70	233	71	Left limb; sunlit obs.
Prometheus	Pr	−1	155	E15	s0449843800	Clear	5/31/1998 0:17	14.0	251.1	90	254	91	Right limb
Prometheus	Pr	−1	155	E15	s0449847913	Clear	5/31/1998 0:58	13.4	283.6	80	300	85	Right limb
Culann	Pr	−20	161	E15	s0449843800	Clear	5/31/1998 0:17	14.0	117.6	45	119	46	Right limb
Culann	Pr	−20	161	E15	s0449847913	Clear	5/31/1998 0:58	13.4	176.1	40	177	40	Right limb
Zamama	Pr	19	172	E15	s0449843800	Clear	5/31/1998 0:17	14.0	200.7	100	255	127	Right limb
Zamama	Pr	19	172	E15	s0449847913	Clear	5/31/1998 0:58	13.4	160.0	40	187	47	Right limb
Ra	Pr	−10	323	G1	s0350029700	Clear	6/30/1996 3:46	10.5	183.5	20	184	20	Left limb
Acala	Pr	12	331	E15	s0449843800	Clear	5/31/1998 0:17	14.0	230.2	50	246	53	Left limb
Acala	Pr	12	331	E15	s0449847913	Clear	5/31/1998 0:58	13.4	247.3	70	286	81	Left limb
Acala	Pr	10	335	G8	s0394394200	Clear	5/6/1997 16:00	18.6	313.9	60	349	67	Left limb
Acala	Pr	10	335	C9	s0401957745	Clear	6/28/1997 18:36	14.6	220.0	40			Disk
Acala	Pr	10	335	C10	s0413546765	Clear	9/18/1997 3:34	13.3	105.0	30	202	58	Left limb
Acala	Pr	10	335	E11	s0420858600	Clear	11/8/1997 11:44	13.7	204.3	65	243	77	Left limb
Culann/Prometheus				G8	s0394394200	Clear	5/6/1997 16:00	18.6	222.4	55			Right limb
Culann/Prometheus				E11	s0420858600	Clear	11/8/1997 11:44	13.7	205.4	40			Right limb
Zamama/Prometheus				E11	s0420361523	Clear	11/4/1997 23:58	17.9	127.0	60			Right limb

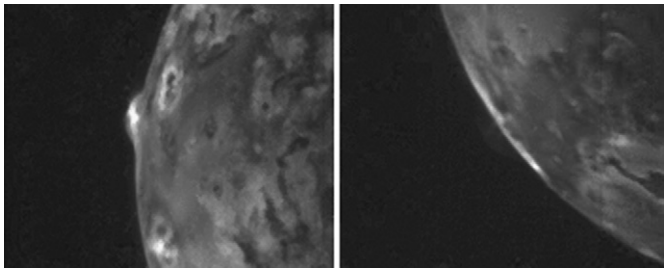

Fig. 3. Comparison of dust columns from Zamama (left) and Marduk (right) under nearly identical illumination and viewing conditions. The opacity of stealthy Marduk is an order of magnitude less than that of similarly sized Zamama.

be confidently associated with particular volcanic eruptive centers. Altogether, 16 observations of 8 different gas plumes met these criteria. The two observations of Thor were not taken in eclipse, but are included here because they are believed to show the extent of the gas plumes, as explained in the next section. Three additional detections of plumes made up of gases from more than one volcanic center are included in Table 2 for completeness.

Fig. 4 shows the distribution of the measured heights of the gas plumes, corrected for foreshortening with the assumption that the location of the source was known in each case. The mean height of the gas jets of Prometheus-type plumes is found to be 258 ± 87 km, considerably larger than the optically thick dust columns. Significantly, we find no consistent difference between the gas plume heights of dusty plumes (such as Zamama or Prometheus) and stealth plumes (Acala and Culann). Acala is much brighter than other Prometheus-type plumes in eclipse, perhaps suggesting a higher gas density from this dust-free plume.

3.3. Contemporaneous gas and dust plume observations

A few Prometheus-type plumes were seen both in daylight and eclipse observations during the same Galileo orbit, giving us

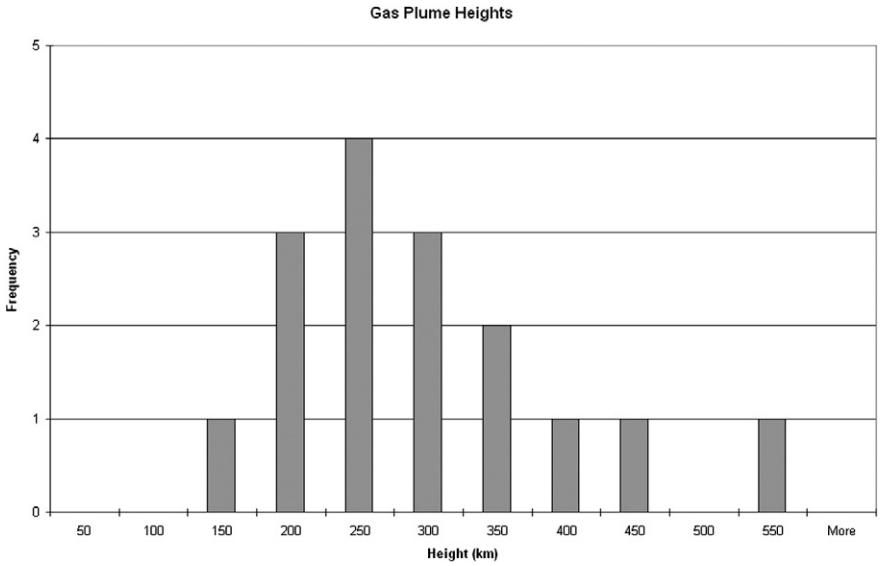

Fig. 4. Histogram of gas column heights. Plumes measured in eclipse included only those with a distinct dome-shaped morphology that were located near known volcanic sources. The mean height of the gas columns of Prometheus-type plumes is 258 ± 87 km, considerably larger than the optically thick dust columns. Significantly, we find similar gas plume heights for dusty plumes (such as Zamama or Prometheus) and stealth plumes (Acala and Culann). The outlier is Grian.

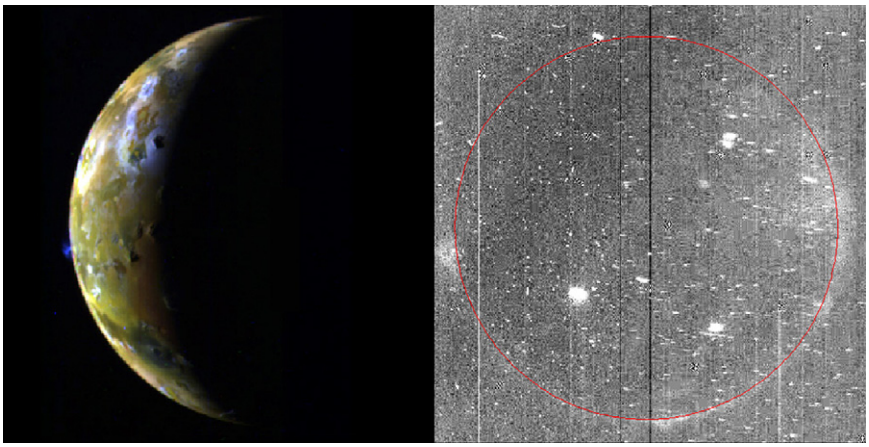

Fig. 5. Ra is shown in images taken in sunlight (left), and again (right) less than an hour later, when Io was in the shadow of Jupiter. The sunlit dust plume from Ra appears obviously smaller than the auroral glow from the gas in eclipse. Galileo orbit G1 images s0350024288ff (left) and s0350029700 (right).

a means to double check the result that the gas plumes are larger than their dusty counterparts. Ra was seen in both daylight and eclipse during orbit G1; Kanehekili was seen during orbit E11; and Prometheus was seen twice, during orbits G8 and E11. These near-contemporaneous observations demonstrate that the Prometheus-type gas plumes are much larger than the optically thick dust plumes, consistent with the statistics given above. Fig. 5 shows images of Ra taken in sunlight (left), and again (right) less than an hour later, when Io was in the shadow of Jupiter. The sunlit dust plume from Ra appears obviously smaller than the auroral glow from the gas in eclipse.

The most compelling indication that the gas plumes exceed the optically thick dust columns in stature comes from a trio of high phase angle, long exposure observations of Thor's eruption during orbit I31 (Fig. 6). Thor's dust plume was overexposed in two of the images, and unfortunately the single unsaturated image was obscured by the spacecraft's magnetometer boom and is uncalibratable. Initially reported as the largest dust plume ever seen on Io, the surface changes produced by the eruption were only slightly broader than typical for Prometheus-type plumes (Geissler et al., 2004a). The surface changes were evidently produced by the optically thick dust column, limited to the bright core close to the surface (pseudocolored red in Fig. 6). The faint outer plume (pale blue in Fig. 6) indicates a second component to the plume, either the gas itself or dust particles small enough to track the gas flow. We will show in Section 4 that the outer envelope must be made up of nm-sized dust particles, possibly related to the clusters of SO_2 molecules inferred from Galileo plasma measurements made as the spacecraft flew within 194 km of the surface of Io just 30 h after the imaging observations were acquired (Frank and Paterson, 2002). In any case, the faint outer halo in Fig. 6 shows that the gas plume of Thor extends much farther than the optically thick dust plume.

3.4. Comparison with surface changes

Having established the range of sizes of the gas plumes and the optically thick dust columns of Prometheus-type plumes, we are now in a position to compare them to the extents of the visible plume deposits in order to determine whether the deposits are produced by the gas or the dust. Fig. 7 (modified from Geissler et al., 2004a) shows a map of the large-scale surface changes detected over the duration of the Galileo mission as demonstrated by differences in surface albedo or color between subsequent SSI im-

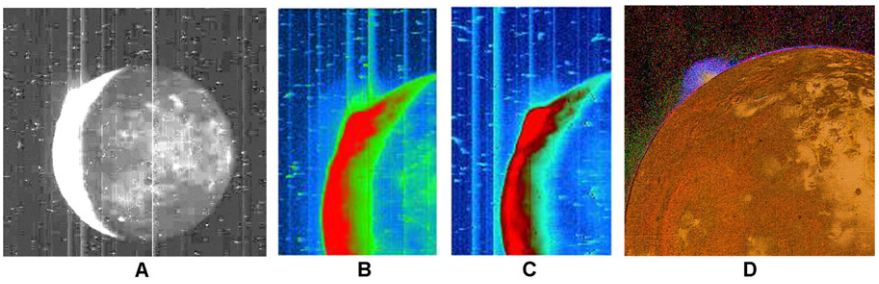

Fig. 6. Thor compared to Loki. Thor's eruption during orbit I31 was captured in a pair of high phase angle, overexposed images that show a faint halo surrounding the optically thick dust column. The surface changes from Thor were evidently produced by the optically thick dust, limited to the bright core close to the surface (pseudocolored red in parts B and C). The faint outer plume (pale blue) indicates a second component to the plume, made up of dust particles small enough to track the gas flow. Similar structure was seen in Loki's plume (part D) in Voyager 1 false color (ultraviolet) images. (A) Galileo image s0615325147. (B and C) PIA02592. (D) PIA01368.

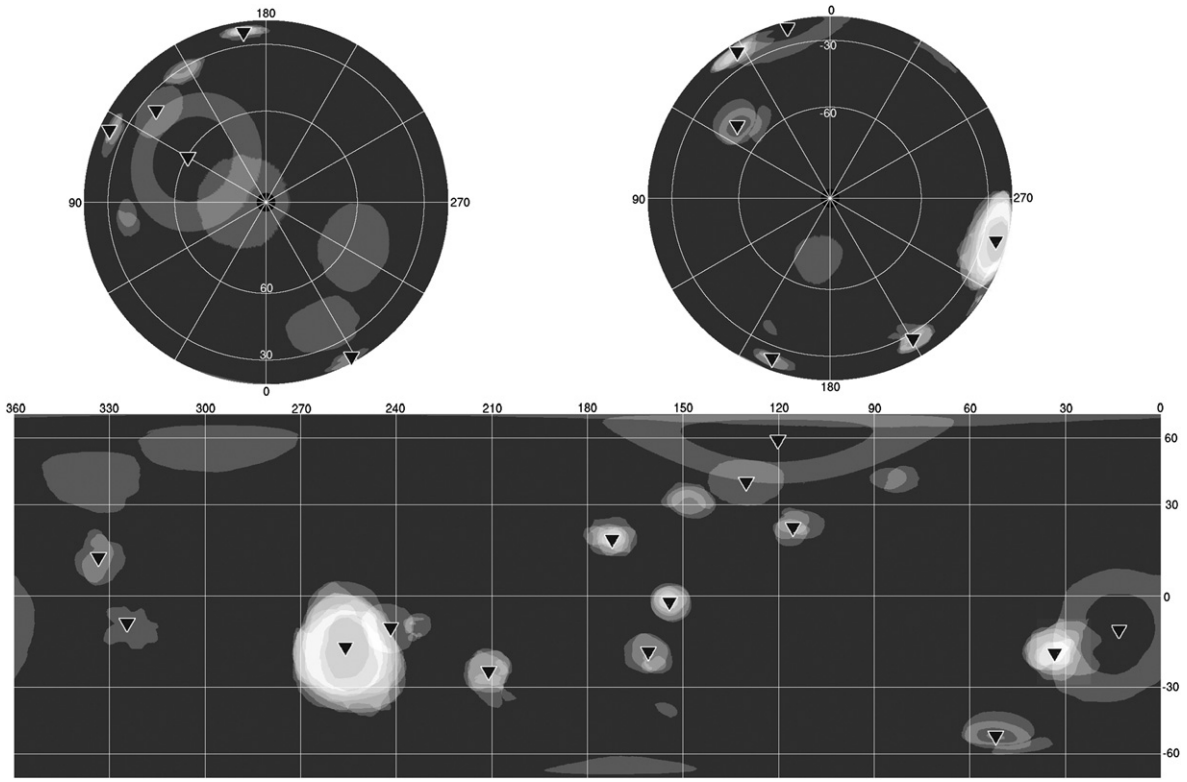

Fig. 7. Locations of plumes and surface changes. Gray zones map the large-scale plume deposits detected by Galileo through changes in surface albedo or color between subsequent SSI images. The brightness of the regions mapped depicts the frequency of deposition, not the deposit thickness. Triangles point out the locations where plumes were spotted during the 5 year period of observation. Surface changes were produced around each of the plumes, including the "stealth" plumes Acala and Culann that went unseen in daylight. In addition, surface changes were seen in several other locations in which plume activity was missed by Galileo. Figure modified from Geissler et al. (2004a).

ages. In this figure, the brightness of the regions mapped depicts the frequency of deposition, not the deposit thickness. Triangles point out the locations where plumes were spotted during the 5 year period of observation; we note that surface changes were produced around each of the plumes, even those like Acala and Culann that went unseen in daylight. In addition, surface changes were seen in several other locations in which plume activity was missed by Galileo.

Fig. 8 shows the distribution of the maximum radial extents of the surface changes. The histogram is bimodal: the larger peak corresponds to Prometheus-type eruptions, while the broad population with extents greater than 350 km corresponds to the giant red rings left by Pele-type plumes. Asterisks mark the maximum ranges of deposits expected from Prometheus-type dust and gas components (twice the heights of the dust and gas plumes, since the maximum radial extent of ballistic deposition is expected to be double the maximum height). The peak of the distribution of observed Prometheus-type plume deposits closely matches the mean maximum range expected from the optically thick dust columns. The surface changes caused by Prometheus-type plumes appear to be produced by dust deposition rather than condensation of gas on the surface.

Here we must emphasize that Figs. 7 and 8 show only the surface changes that were apparent at visible wavelengths to the SSI camera. The infrared imaging spectrometer (NIMS) showed evidence for patches of SO_2 frost that were transparent at visible wavelengths and invisible to SSI (Doute et al., 2001).

3.5. Giant plumes

Galileo images of giant plumes are limited to two marginal detections of Pele in sunlight and a possible detection of a plume from Grian (south of Karei) in eclipse. Pele's faint outline was seen during daytime on orbit E4, more than 400 km high and at least

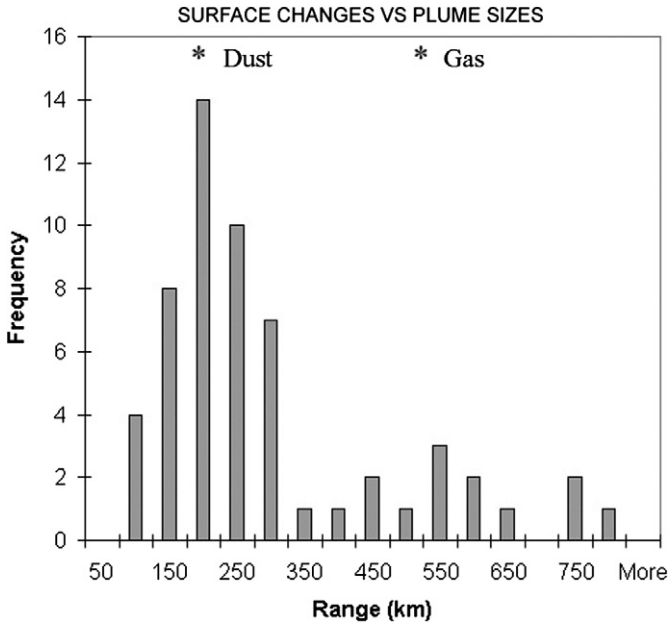

Fig. 8. Dimensions of surface changes seen by Galileo compared to the expected range of Prometheus-type dust and gas particles. The histogram of surface change extents is bimodal, corresponding to Prometheus-type plume deposits (<350 km) and the giant red rings from Pele-type plumes (>350 km). Asterisks mark the maximum ranges of deposits expected from Prometheus-type dust and gas components (twice the heights of the dust and gas columns, since the maximum radial extent of ballistic deposition is expected to be double the maximum height). The expected extent of deposition from the optically thick dust closely matches the mean range of Prometheus-type surface changes (the larger peak in the histogram, with extents less than 350 km). This correspondence suggests that the surface changes caused by Prometheus-type plumes are produced by dust deposition rather than condensation of gas on the surface.

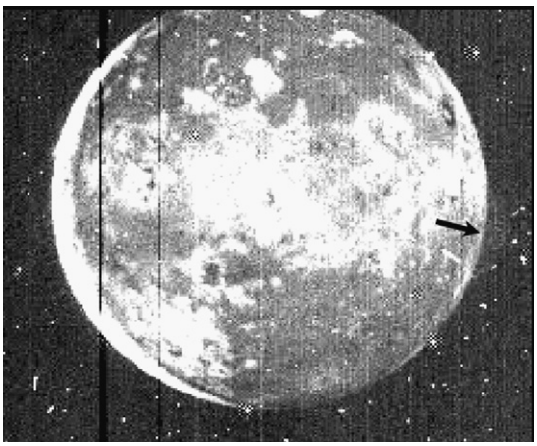

Fig. 9. Pele in sunlight. Pele's faint outline (arrow) was barely detected during daytime on orbit E4, more than 400 km high and at least 800 km across. Image s0374850023.

800 km across (Fig. 9). Pele was spotted once more in daylight on orbit G29. Higher resolution Voyager images of Pele in sunlight show a shield-shaped structure more than 1100 km across with only a faint central column (Strom et al., 1981). The eclipse observation taken during orbit C21 shows a faint glow from a region near the Jupiter-facing point where a giant red ring was briefly deposited by an eruption of Grian at 12 S, 13 W (Fig. 10). The gas plume here is ~500 km high and 1100 km across, matching the breadth of the red ring left by the eruption.

The dearth of detections of giant plumes by Galileo is significant, considering the quasi-continuous eruptions of Pele during the mission and sporadic eruptions of Grian, Tvashtar, Surt and

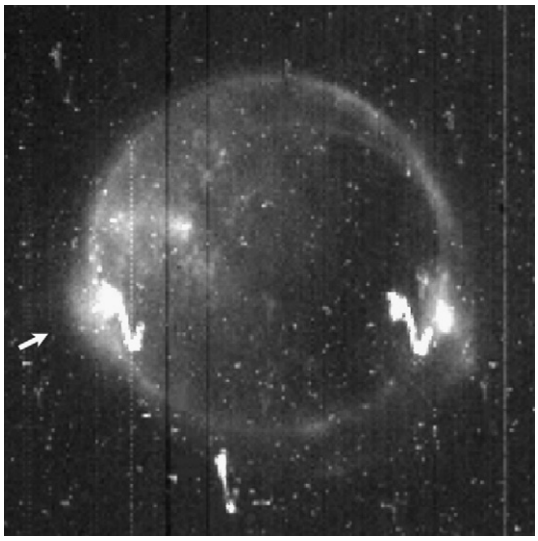

Fig. 10. Grian in eclipse. This eclipse observation taken during orbit C21 shows a bright hot spot and a faint atmospheric glow (arrow) from a region near the Jupiter-facing point where a giant red ring was briefly deposited by an eruption centered at 12 S, 13 W. The gas plume here is ~500 km high and 1100 km across, matching the breadth of the red ring left by the eruption. Image s0506570500. Because of its location on the left side of the image, the plume outline is unaffected by the smear produced by camera motion while the shutter was open.

an unnamed volcanic center near 80 N, 100 W that all deposited fresh, giant, red rings on the surface. Plumes from Tvashtar and Pele were both seen at low resolution by Cassini as it flew past the Jupiter system en route to Saturn in late 2000 (Porco et al., 2003). The best images of Pele's dust plume remain those taken by Voyager 1. The reason that Cassini and Voyager could image the giant plumes is that their imaging systems were sensitive to ultraviolet wavelengths, a capability that Galileo lacked. This tells us that the dust particles in giant plumes are much finer than those of the optically thick dust columns from Prometheus-type plumes.

Based on the available images from Voyager, Galileo, and Cassini, we can draw a few conclusions about the giant plumes in general. First, the gas jets, dust columns, and surface deposits all appear comparable in size and much larger than those of Prometheus-type plumes. Second, the giant plumes have a characteristic shield-shaped morphology that differs from the smaller plumes in the lack of a dense central core. Third, the dust particles that make up the giant plumes are extremely faint in scattered sunlight at visible wavelengths, indicating that the particle sizes are much smaller than those of the optically thick Prometheus-type plumes.

3.6. Other plumes

Diffuse glows were spotted in the vicinity of a poorly resolved field of hot spots on the leading side of Io near the sub-Jupiter point, especially during the eclipse observation of orbit C10 (image s0413546765). These emissions could indicate venting of gas from extended sources or from multiple volcanic centers too weak to be detected as individual plumes. During this same orbit, Grian, one of the volcanic centers in this region, produced a small puff of red smoke that was barely detected by Galileo, as described in Section 3.7. It is thus possible that Grian contributed to the gas that was seen in this region during eclipse.

3.7. Plume colors

The diversity of colors displayed by Prometheus-type dust plumes in daylight adds another level of complexity to the plume

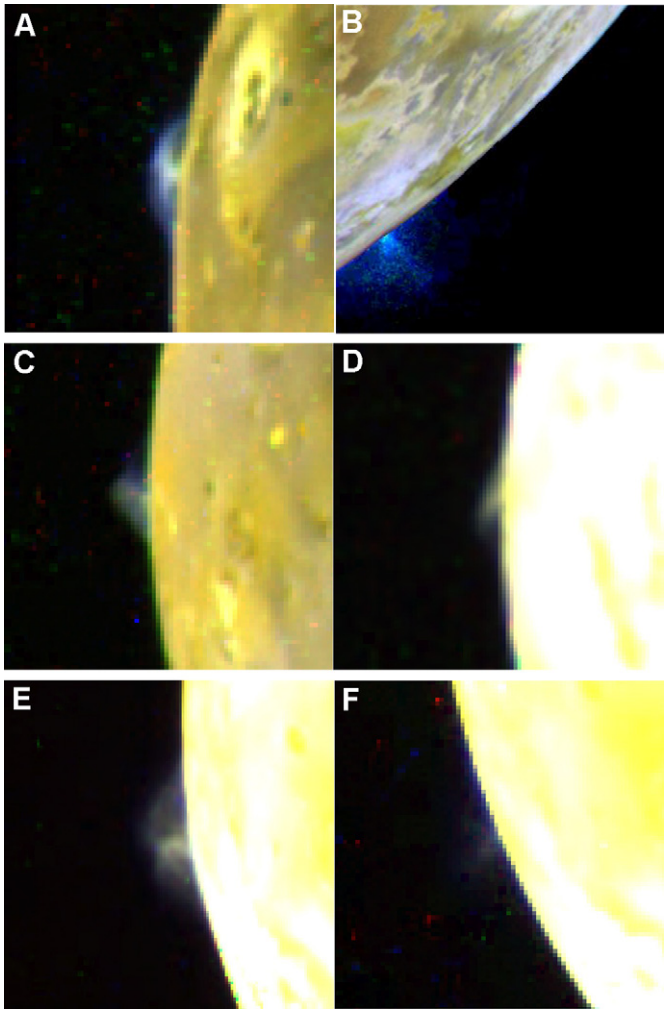

Fig. 11. Colors of Prometheus-type dust columns. (A) Zamama orbit E11. (B) Masubi orbit C21 (false color, Violet and 756 nm filters); PIA02502. (C) Prometheus orbit G8. (D) Prometheus orbit C9. (E) Pillan orbit C9. (F) Pillan orbit E11. Except for Masubi, the images are contrast-stretched linearly to show color differences. Prometheus and Pillan both appeared yellow during orbit C9, in contrast to the more typical blue hues of the plumes.

story. Most of the optically thick dust columns are blue in color, contrasting sharply with the yellows and reds of Io's surface. This indicates that the dust particles are smaller than or comparable in size to the wavelength of visible light, as explained in the next section. However, there are some notable exceptions to this general rule, and variations in color over time scales of weeks were noted even in observations of the same plumes.

Fig. 11 shows the variety of colors sported by Prometheus-type dust columns. Zamama (Fig. 11A) exemplifies the typical hue of the dust plumes; Zamama remained consistent in color throughout the Galileo observations, irrespective to first order of variations in incidence, emission, or phase angle. Masubi (Fig. 11B) was seen in false color (Violet and 756 nm filters) at a resolution in Violet of 3.2 km/pixel. Prometheus (Figs. 11C, 11D) appeared similar in color to Zamama except during orbit C9, when it was brighter than usual and yellow rather than blue, indicating coarser dust grains. Pillan (Figs. 11E, 11F) was yellow when it first erupted but reverted to a more typical blue in the waning stages of the eruption. Pillan's dense plume produced an unusual black deposit on the surface, obscuring a portion of Pele's red ring. This indicates that silicates were entrained in Pillan's dust plume. One other dubious detection of an unusually colored plume was that of Grian in orbit C10. A faint smudge was seen near the limb of Io in the Red and 756 nm filter images but was not visible in the sharper Violet and Green images. It is possible that this observation represents a conspiracy of compression artifacts, but it is included in Table 1 because a giant red ring erupted from Grian two years later during orbit C21, and we cannot rule out the possibility that red dust was exhaled from the volcano as a precursor to the later explosion.

Fig. 12 shows our measurements of the spectra of individual plumes, in units of reflectance (I/F). There is a great deal of variability in plume brightness and color, but in general the reflectance of the optically thick dust columns tends to be higher at shorter wavelengths. Fig. 13 shows the mean color of the most reliable dust column observations, excluding the exceptional yellow and red plumes discussed earlier. Here we have normalized the measurements to the Violet filter reflectance, to compensate for brightness variations from one observation to another, and then averaged the resulting ratios. This is the spectrum of "typical" plumes that we will seek to match with theoretical calculations in the next section. One additional observation of importance is that there is little apparent variation of color with phase angle, as shown in Fig. 14.

3.8. Summary of observations

Galileo observations of volcanic plumes on Io reveal a zoo of individuals with different sizes, morphologies, colors, and opacities. The following features must be explained by any comprehensive theory that seeks to explain the diversity of Io's explosive eruptions: (1) the optically thick dust columns of Prometheus-type plume decouple from the gas flow and fall short of the extent of the gas plumes that drive them (gas plumes are ∼3 times larger than the optically thick dust plumes); (2) refractory materials like silicates can sometimes be entrained in the dust from Prometheus-type plumes; (3) the dust loads of Prometheus-type plumes are independent of plume height (initial gas temperature), as expected for entrained particles; (4) the visible surface changes produced by Prometheus-type plumes are consistent with the trajectory of the dust, and not that of the gas; (5) a fine-grained population of particles that follows the gas flow can be seen in long exposure images of certain Prometheus-type plumes like Thor; (6) Pele-type giant plumes have similarly sized dust columns, gas plumes and surface deposits, implying a lack of separation of the gas and dust components; and (7) Pele-type plumes lack a distinct central core, consistent with the possibility that the dust particles are condensed directly from the gas.

4. Interpretation

To estimate particle sizes and plume masses, we used the publicly available program Mieplot by Philip Laven (www.philiplaven.com). Mieplot provides a choice of Mie, Rayleigh, and other scattering laws and outputs predicted intensity as a function of wavelength and optical power as a function of scattering angle. It allows for a distribution of particle sizes, which is important because of the strong wavelength- and scattering-angle-dependence predicted for particular particle sizes. For our simulations, we assumed a normal distribution of dust grain radii with a standard deviation of 20% about the mean. The modeling results reported here are most appropriate to liquid droplets; crystals and complex aggregates such as snowflakes are not well modeled by spherical scatterers. We assumed the refractive index of liquid SO_2 (1.34; Musso et al., 2000) but the conclusions are little changed over a range of refractive indices from 1.3 to 1.9 (appropriate to H_2O and S, respectively).

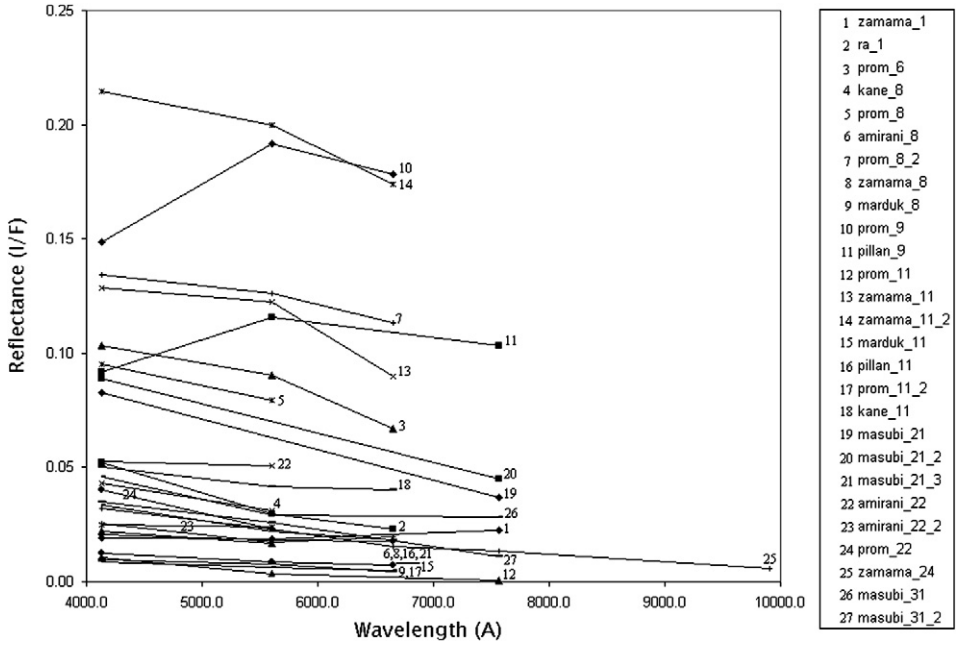

Fig. 12. Spectra of Prometheus-type dust plumes, in units of reflectance (I/F). There is a great deal of variability in plume brightness and color, but in general the reflectance of the optically thick dust columns is higher at shorter wavelengths. Notable exceptions are Prometheus and Pillan, which both appeared yellow during orbit C9 (cf. Fig. 11).

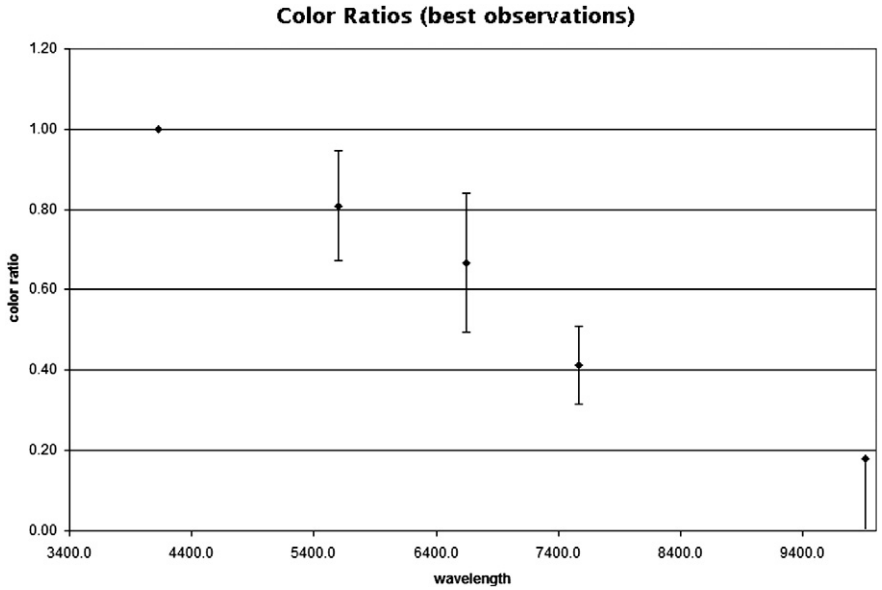

Fig. 13. Mean color of Prometheus-type dust plumes. This figure shows the spectrum of the optically thick dust columns that were best observed by Galileo's camera, excluding the exceptionally colored red and yellow plumes. The measurements were normalized to the Violet filter reflectance, to compensate for brightness variations from one observation to another, and the resulting ratios were then averaged. The point at 9680 Å is an upper limit.

4.1. Dust particle sizes

Particles that are very small or very large in comparison to the wavelength are inefficient scatterers of sunlight, so the visibility of plumes is strongly affected by the wavelength of the observations. Moreover, the estimated mass of plumes depends sensitively on the grain size assumed. We used the plume color measurements described previously in Section 3.7 to establish the mean grain size of the optically thick dust plumes. Both Rayleigh and Mie theory predict a λ^{-4} dependence of scattered light intensity for particles with radii $r \ll \lambda$. As we have seen, the plume colors recorded by Galileo SSI display an approximately linear decrease in intensity over the wavelength interval from 410 nm to 756 nm. These observations rule out very small particles (1 nm to 10 nm) as the dominant scatterers in the optically thick dust columns. Instead, the simulations suggest that scattering in the dust plumes is dominated by particles that are smaller than, but comparable to, the wavelength of visible light. The best fits to the Galileo color observations are obtained with particle radii in the range 80 nm to 120 nm, depending on the scattering angle (Fig. 15). The model fits are imperfect, however; theory predicts some variations in color with scattering angle that are not seen in the observational data of Fig. 14. We conclude from these simulations that (1) nanometer-sized particles do not dominate the scattering of visible light by the optically thick dust columns; (2) the dust grains that contribute most to the scattering seen by Galileo SSI are smaller than but comparable to the wavelength of visible light (i.e., in the radius range of 80 nm to 120 nm); and (3) the distri-

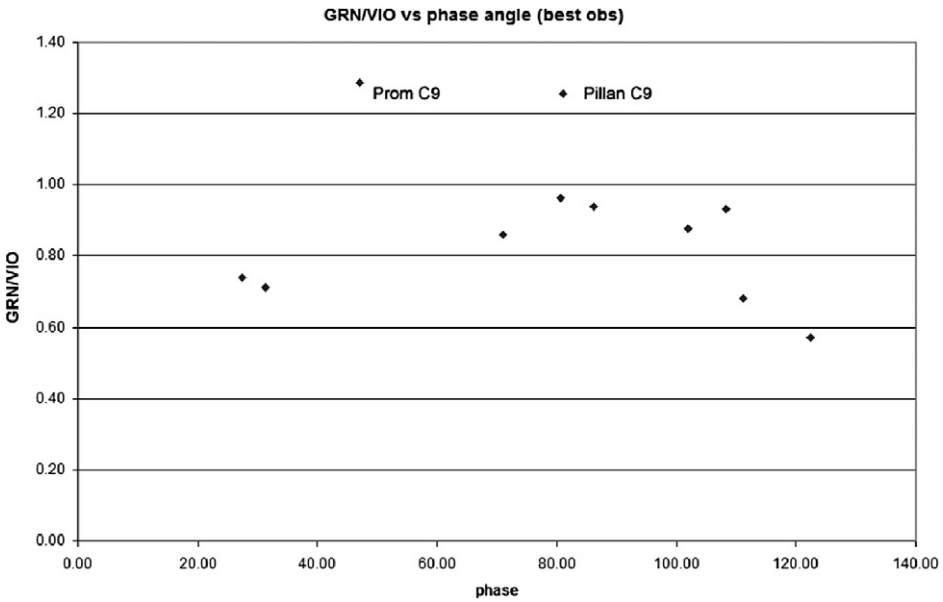

Fig. 14. Dust column color vs phase angle. The best observed Prometheus-type dust plumes show little variation of color ratio (Green/Violet reflectance) with phase angle, an important constraint for scattering models.

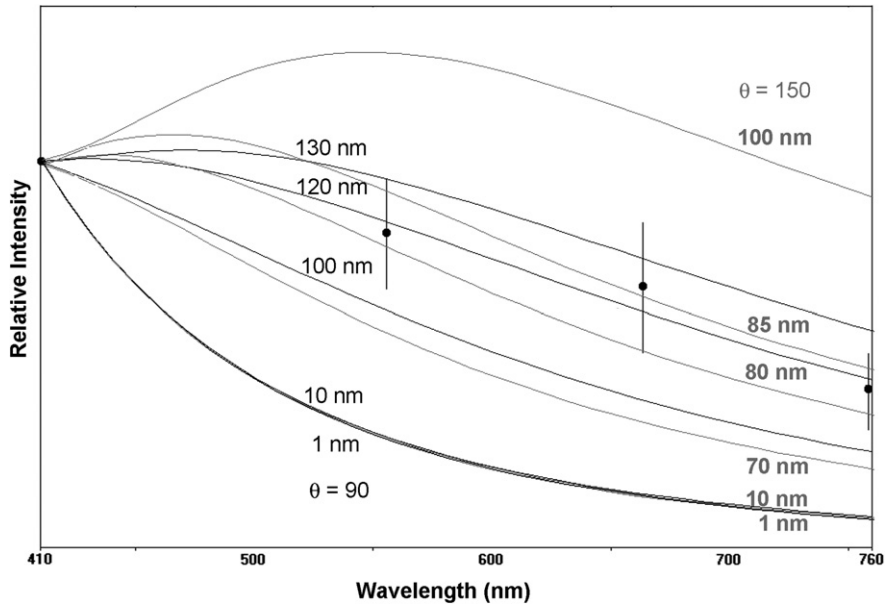

Fig. 15. Mie scattering predictions compared to observed dust plume color. Simulations suggest that scattering in the optically thick Prometheus-type dust plumes is dominated by particles that are smaller than, but comparable to, the wavelength of visible light. The best fits to the Galileo color observations are obtained with particle radii in the range 80 nm to 120 nm, depending on the scattering angle. The darker curves are computed for a scattering angle of 90 degrees, while the lighter toned curves are for a scattering angle of 150 degrees. Data points are from Fig. 13.

bution of grain sizes, the grain shapes, or the optical properties of the dust grains are more complex than the simple approximations used here.

4.2. Dust plume masses

Dust plume masses were estimated by calculating the optical power ($W\,m^{-2}$) predicted of scattering by a single sphere and comparing that to the total optical power observed from a plume. Several quantities are needed for this calculation. The plume's total optical power is measured as the mean spectral radiance ($W\,m^{-2}\,sr^{-1}\,nm^{-1}$), times the solid angle per pixel, times the number of pixels subtended by the plume, times the filter bandwidth. The incident flux was estimated by scaling the Standard Extraterrestrial Reference Spectrum (ASTM, 2000) over each filter bandpass to Jupiter's distance by dividing by 5.2^2. The distance between the spacecraft and the target was read from the image labels. We assumed that the dust particles were spheres of liquid SO_2 with radii of 120 nm to conservatively estimate plume masses.

Table 3 lists the masses of the optically thick dust columns estimated in this way. The typical mass of the visible plumes is of order 10^6 kg. Assuming a mean dynamical lifetime (time of flight) of 10^3 s, these masses imply dust production rates of order 10^3 $kg\,s^{-1}$. The variability of dust plume masses is about a factor of 10, similar to the range of plume opacities. However, there is no straightforward relationship between plume mass and reflectivity because the mass estimate depends also on the scattering

Table 3
Masses of entrained dust in Prometheus-type plumes

Name	Lat.	Lon.	Orbit	Image	Filter	GMT (M/D/Y H:M)	Res. (km/pix)	Scattering angle	Measured W/m^2	Expected W/m^2 (1 particle)	# of particles	Mass (kg)
Ra	−10	323	G1	s0350024288	Violet	6/29/1996 2:50	9.85814	57.5	2.90E−10	1.15E−32	2.52E+22	2.67E+05
Kanehekili	−19	34	G8	s0394435001	Violet	5/6/1997 22:52	12.9877	109.1	4.54E−10	7.40E−34	6.13E+23	6.48E+06
Prometheus	−1	155	G8	s0394505123	Violet	5/7/1997 10:41	9.99294	93.8	1.47E−09	1.70E−33	8.67E+23	9.17E+06
Prometheus	−1	155	C9	s0401785407	Violet	6/27/1997 13:33	8.29211	132.9	1.65E−09	1.00E−33	1.65E+24	1.74E+07
Pillan	−11	242	C9	s0401863204	Violet	6/28/1997 2:40	6.15029	99	2.91E−09	3.40E−33	8.56E+23	9.05E+06
Prometheus	−1	155	E11	s0420730085	Violet	11/7/1997 14:05	9.27637	78.2	1.034E−09	4.40E−33	2.349E+23	2.48E+06
Zamama	19	175	E11	s0420743485	Violet	11/7/1997 16:20	8.9706	71.8	1.868E−09	7.60E−33	2.457E+23	2.60E+06
Marduk	−23	211	E11	s0420773085	Violet	11/7/1997 21:19	8.19641	66.4	1.359E−10	1.20E−32	1.133E+22	1.20E+05
Masubi	−44	54	C21	s0506406153	Violet	7/2/1999 4:05	3.26227	174.8	1.27E−08	6.70E−32	1.90E+23	2.01E+06
Amirani	21	112	C22	s0512436223	Violet	8/13/1999 12:15	16.3901	99.3	2.78E−10	4.80E−34	5.784E+23	6.11E+06

angle of the observations (lower phase implies higher mass for the same I/F).

More difficult to constrain but potentially far more significant is the mass of the faint outer halo of Thor. We can rule out Rayleigh scattering by gas molecules as an explanation for the halo, following the argument of Collins (1981). Citing McCartney (1976), Collins gives the column density of a Rayleigh scattering gas as

$$N_L = \frac{2N_0^2\lambda^4}{\pi^3(n^2-1)^2(1+\cos^2\theta)} \times I/F,$$

where N_0 is Loschmidt's number (2.687×10^{25}), and n is the refractive index of SO_2 vapor at STP (1.000686; Kaye and Laby, 1995). Our measured I/F of 0.0007, although much smaller than that measured by Collins (1981) for Loki, still requires a column density of 3×10^{22} cm^{-2}, or about 10 m amagat of gas, and a total plume mass of gas at Thor of order 10^{13} kg. This is unreasonably large in comparison to estimates of plume gas column densities based on SO_2 absorption band depths (Jessup et al., 2004) or auroral emission intensities (Geissler et al., 2004b), which are in the range 10^{16} to 10^{17} cm^{-2}.

A more plausible explanation is that Thor's halo is produced by fine dust grains small enough to be carried along with the gas flow. Tiny particles with masses in the range of 500 to 1000 amu were in fact detected by the Galileo plasma instrument (PLS) as the spacecraft brushed within 200 km of Io's northern polar surface a day after Thor's plume was spotted erupting in the same hemisphere (Frank and Paterson, 2002). Lacking color information, we suppose the particle size of these fine particles to be between 0.5 nm (the radius of a compact sphere made up of 10 SO_2 molecules, the middle of the range of particle masses inferred from the PLS measurements) and 10 nm (the largest dense dust grain that can be carried along in suspension by the plume gas; Zhang et al., 2004). The minimum mass of the halo would be obtained in the case of fine dust grains that are made up of fluffy aggregates with a large effective physical size but relatively low density. For example, if we assume 10 nm radius particles with a density one quarter that of liquid SO_2, we calculate a total mass of fine particles within Thor's halo of 10^8 kg. Less extreme assumptions lead to even higher masses for these nearly invisible particles. We conclude in any case that the nm-sized particles making up Thor's faint outer plume comprise far more mass than the optically thick dust core.

5. Discussion

The singular observations of Thor both point out the shortcomings of the Galileo visible images of Io's plumes and also explain the discrepancy between the Galileo results and those of Collins (1981), based on Voyager visible and ultraviolet observations. The Voyager images showed that Loki's dust plume was made up of two components: a coarse grained core and an outer envelope of finer particles that was much more massive (Fig. 6D). Almost all of the Galileo images were acquired with short exposure times to prevent saturation of the illuminated surface of Io, and all were taken in visible or near-infrared passbands. For these reasons, Galileo may have only detected the central cores of the dust plumes and missed the fine particulates that make up most of the mass of plume dust.

The two components of dust plumes seem to require two distinct mechanisms for generating dust particles. The dense central columns of Prometheus-type plumes, the relatively large size of the particles, the inclusion of refractory silicates, and the lack of correlation between dust content and gas temperature are all consistent with an origin of the coarse grained dust as liquid or solid "ash" that is entrained with the gas flow as it erupts from the surface. In contrast, the fine particles that make up the outer haloes of Thor and Loki could be sulfurous "snowflakes" condensed from the gas phase after eruption, as the gas expands and cools adiabatically and by radiation. Similarly, the fine dust associated with the giant Pele-type plumes may be generated by condensation at the shock front, explaining the shield-like shapes of the giant plumes and the lack of a distinct central core.

The coarse-grained ash entrained by Prometheus-type plumes comprises less than 10% of the mass of the gas, according to estimates of gas plume mass by Jessup et al. (2004). The coarse grained dust production rates implied by our measurements are sufficient to produce the visible surface changes observed near the plumes; a deposit ~100 μm thick would be laid down by Zamama or Prometheus over a 2 month period (the typical interval between Galileo imaging observations), and a layer 3 mm thick would be deposited over the 5 year duration of the mission. However, this rate of deposition is insufficient to account for the rapid resurfacing of Io, estimated at ~1 mm/yr, globally averaged (Spencer and Schneider, 1996). The power expended by the plumes in lofting the ash, $(1/2)\dot{m}v^2$, amounts to more than 10^8 W per plume, or at least 10^9 W globally. Even including the much more massive gas, the power dissipated globally by Io's plumes (10^{10} W) is a small fraction of Io's total energy budget from tidal heating (10^{14} W).

Among the important outstanding questions concerning the plumes is whether faint haloes of fine, nearly invisible particles are common features of Prometheus-type plumes. The Voyager observations of Loki, which was exceptionally tall for an otherwise typical Prometheus-type plume issuing from the toe of a lava flow, would seem to suggest that this might be the case. More observations with long exposure times, high phase angles, and short wavelengths are needed to resolve this question. Another way to approach the problem might be to carefully compare the Galileo SSI images of surface deposits with the data from Galileo's infrared imaging spectrometer (NIMS), looking for evidence of SO_2 frost deposits made up of nanometer sized particulates (or directly condensed onto the surface from the gas phase). Yet another set of questions concerns the giant, Pele-type plumes, about which Galileo provided little information. What is particle size of Pele's dust? How massive are the giant dust plumes? Does it snow sul-

fur on Io? The data from Voyager, Cassini, and New Horizons will be needed to discern the nature of the giant plumes and their role in Io's resurfacing.

6. Conclusions

Our study has shown that there is more to Io's mysterious plumes than meets the eye, found answers to some of the questions posed earlier, and raised new questions to be addressed by other observations and data sets. The main findings of this work can be summarized as follows.

1. *Source of the dust particles*. Prometheus-type plumes possess two distinct dust components. The first component is coarse grained "ash" that is evidently entrained with the gas upon eruption but falls short of the gas flow, is optically thick at visible wavelengths (indicating particles that are comparable in size to the wavelength of visible light), varies in number density independently of the gas column height (i.e., the temperature of the gas), and may include refractory components such as silicates. The second component is fine grained dust spotted in some Prometheus-type plumes such as Thor and Loki that is small enough ($r < 10$ nm) to be carried along with the gas flow, and could represent SO_2 "snowflakes" condensed from the gas phase.
2. *Cause of the surface changes*. The visible surface changes produced by Prometheus-type plumes on Io are caused by the coarse grained ash columns that are optically thick at visible wavelengths. This result applies strictly to the plume deposits documented in SSI images by Geissler et al. (2004a); it does not rule out surface condensation from the gas phase or deposition of fine particles that may produce frosts of SO_2 that are transparent at visible wavelengths.
3. *Mass of plume dust*. The mass of coarse grained ash entrained by an individual Prometheus-type plume is typically 10^6 kg, implying ash production rates of $\sim 10^3$ kg s^{-1} per plume. The ash comprises only $<10\%$ of the mass of the gas. In contrast, the fine dust suspended by Thor comprises at least 10^8 kg, comparable to the mass of the gas (assuming that Thor's gas column density was equal to that of Prometheus).
4. *Significance for resurfacing*. Despite their spectacular appearance, the optically thick ash columns from Prometheus-type plumes are responsible for only a small fraction of the resurfacing of the satellite. The erasure of impact craters must be achieved either by the emplacement of lava flows or by more subtle deposition from the plumes that was missed by Galileo's camera, such as SO_2 snowfall or direct condensation from the gas phase onto the surface. More analysis of observations from instruments other than Galileo SSI are needed to quantify the importance of these alternate deposition mechanisms.
5. *Giant plumes*. Limited information about the Pele-type plumes from Galileo SSI suggests that the gas plumes, dust columns, and surface changes are all similarly sized, indicating that the gas and dust components of giant plumes do not separate. The poor visibility of Pele's dust is another indication that the particles must be much smaller than those of the dust columns from Prometheus-type plumes. Together, these facts admit the possibility that it snows (or rains) sulfur from Io's giant plumes.

Acknowledgments

The authors wish to thank Lori Feaga and Kandis Lea Jessup for constructive comments on an earlier draft of this manuscript. We are grateful to John Spencer for pointing out the plume of Pele in orbit G29 images.

References

ASTM, 2000. Standard Extraterrestrial Reference Spectrum. American Society for Testing and Materials Standards, West Conshohocken, PA.

Cataldo, E., Wilson, L., Lane, S., Gilbert, J., 2002. A model for large-scale volcanic plumes on Io: Implications for eruption rates and interactions between magmas and near-surface volatiles. J. Geophys. Res. 107 (E11), doi:10.1029/2001JE001513. 5109.

Collins, S.A., 1981. Spatial color variations in the volcanic plume at Loki, on Io. J. Geophys. Res. 86, 8621–8626.

Doute, S., Schmitt, B., Lopes-Gautier, R., Carlson, R., Soderblom, L., Shirley, J., The Galileo NIMS Team, 2001. Mapping SO_2 frost on Io by the modeling of NIMS hyperspectral images. Icarus 149, 107–132.

Frank, L.A., Paterson, W.R., 2002. Plasmas observed with the Galileo spacecraft during its flyby over Io's northern polar region. J. Geophys. Res. (Space Phys.) 107, doi:10.1029/2002JA009240. 31-1.

Gaddis, L., Anderson, J., Becker, K., Becker, T., Cook, D., Edwards, K., Eliason, E., Hare, T., Kieffer, H., Lee, E.M., Mathews, J., Soderblom, L., Sucharski, T., Torson, J., McEwen, A., Robinson, M., 1997. An overview of the Integrated Software for Imaging Spectrometers (ISIS). Lunar Planet. Sci. 28, 387.

Geissler, P.E., McEwen, A.S., Ip, W., Belton, M.J.S., Johnson, T.V., Smyth, W.H., Ingersoll, A.P., 1999. Galileo imaging of atmospheric emissions from Io. Science 285, 870–874.

Geissler, P.E., Smyth, W.H., McEwen, A.S., Ip, W., Belton, M.J.S., Johnson, T.V., Ingersoll, A.P., Rages, K., Hubbard, W., Dessler, A.J., 2001a. Morphology and time variability of Io's visible aurora. J. Geophys. Res. 106, 26137–26146.

Geissler, P., McEwen, A., Phillips, C., Simonelli, D., Lopes, R.M.C., Douté, S., 2001b. Galileo imaging of SO_2 frosts on Io. J. Geophys. Res. 106, 33253–33266.

Geissler, P., McEwen, A., Phillips, C., Keszthelyi, L., Spencer, J., 2004a. Surface changes on Io during the Galileo mission. Icarus 169, 29–64.

Geissler, P., McEwen, A., Porco, C., Strobel, D., Saur, J., Ajello, J., West, R., 2004b. Cassini observations of Io's visible aurorae. Icarus 172, 127–140.

James, M.R., Wilson, L., 1998. An optical model for ballistic plumes on Io. Lunar Planet. Sci. 29, 1349.

Jessup, K.L., Spencer, J.R., Ballester, G.E., Howell, R.R., Roesler, F., Vigel, M., Yelle, R., 2004. The atmospheric signature of Io's Prometheus plume and anti-jovian hemisphere: Evidence for a sublimation atmosphere. Icarus 169, 197–215.

Johnson, T.V., Soderblom, L.A., 1982. Volcanic eruptions on Io—Implications for surface evolution and mass loss. In: Morrison, D. (Ed.), Satellites of Jupiter. Univ. of Arizona Press, Tucson, pp. 634–646.

Johnson, T.V., Matson, D.L., Blaney, D.L., Veeder, G.J., Davies, A., 1995. Stealth plumes on Io. Geophys. Res. Lett. 22, 3293–3296.

Kaye, G.W.C., Laby, T.H., 1995. Tables of Physical and Chemical Constants, 16th ed. (online). National Physical Laboratory, Essex, UK.

Keszthelyi, L., McEwen, A.S., Phillips, C.B., Milazzo, M., Geissler, P., Turtle, E.P., Radebaugh, J., Williams, D.A., Simonelli, D.P., Breneman, H.H., Klaasen, K.P., Levanas, G., Denk, T., Galileo SSI Team, 2001. Imaging of volcanic activity on Jupiter's moon Io by Galileo during the Galileo Europa Mission and the Galileo Millennium Mission. J. Geophys. Res. 106, 33025–33052.

Kieffer, S.W., 1982. Dynamics and thermodynamics of volcanic eruptions: Implications for the plumes of Io. In: Morrison, D. (Ed.), Satellites of Jupiter. Univ. of Arizona Press, Tucson, pp. 647–723.

Klaasen, K.P., Belton, M.J.S., Breneman, H.H., McEwen, A.S., Davies, M.E., Sullivan, R.J., Chapman, C.R., Neukum, G., Heffernan, C.M., Harch, A.P., Kaufman, J.M., Merline, W.J., Gaddis, L.R., Cunningham, W.F., Helfenstein, P., Colvin, T.R., 1997. Inflight performance characteristics, calibration, and utilization of the Galileo SSI camera. Opt. Eng. 36, 3001–3027.

McCartney, E.J., 1976. Optics of the Atmosphere (Scattering by Molecules and Particles). John Wiley and Sons, New York.

McEwen, A.S., Soderblom, L., 1983. Two classes of volcanic plumes on Io. Icarus 58, 197–226.

McEwen, A.S., Keszthelyi, L., Geissler, P., Simonelli, D.P., Carr, M.H., Johnson, T.V., Klaasen, K.P., Breneman, H.H., Jones, T.J., Kaufman, J.M., Magee, K.P., Senske, D.A., Belton, M.J.S., Schubert, G., 1998. Active volcanism on Io as seen by Galileo SSI. Icarus 135, 181–219.

Musso, M., Aschauer, R., Asenbaum, A., Vasi, C., Wilhelm, E., 2000. Interferometric determination of the refractive index of liquid sulfur dioxide. Meas. Sci. Technol. 11, 1714–1720.

Porco, C.C., West, R.A., McEwen, A., Del Genio, A.D., Ingersoll, A.P., Thomas, P., Squyres, S., Dones, L., Murray, C.D., Johnson, T.V., Burns, J.A., Brahic, A., Neukum, G., Veverka, J., Barbara, J.M., Denk, T., Evans, M., Ferrier, J.J., Geissler, P., Helfenstein, P., Roatsch, T., Throop, H., Tiscareno, M., Vasavada, A.R., 2003. Cassini imaging of Jupiter's atmosphere, satellites, and rings. Science 299, 1541–1547.

Spencer, J.R., Schneider, N.M., 1996. Io on the eve of the Galileo Mission. Annu. Rev. Earth Planet. Sci. 24, 125–190.

Spencer, J.R., Sartoretti, P., Ballester, G.E., McEwen, A.S., Clarke, J.T., McGrath, M.A., 1997. Pele plume (Io): Observations with the Hubble Space Telescope. Geophys. Res. Lett. 24, 2471–2474.

Strom, R.G., Schneider, N.M., 1982. Volcanic eruption plumes on Io. In: Morrison, D. (Ed.), Satellites of Jupiter. Univ. of Arizona Press, Tucson, pp. 598–633.

Strom, R.G., Schneider, N.M., Terrile, R.J., Cook, A.F., Hansen, C., 1981. Volcanic eruptions on Io. J. Geophys. Res. 86, 8593–8620.

Turtle, E.P., Keszthelyi, L.P., McEwen, A.S., Radebaugh, J., Milazzo, M., Simonelli, D.P., Geissler, P., Williams, D.A., Perry, J., Jaeger, W.L., Klaasen, K.P., Breneman, H.H., Denk, T., Phillips, C.B., 2004. The final Galileo SSI observations of Io: Orbits G28–I33. Icarus 169, 3–28.

Zhang, J., Goldstein, D.B., Varghese, P.L., Trafton, L.M., Miki, K., Moore, C., 2004. Numerical modeling of ionian volcanic plumes with entrained particulates. Icarus 172, 479–502.